Received: 1 February 2021 | Revised: 23 April 2021 | Accepted: 27 April 2021

DOI: 10.1002/nano.202100053

RESEARCH ARTICLE

Nano Select Open Access WILEY

Two-dimensional oxide based pressure sensors with high sensitivity

Hao Liu[1] | **Bo Feng**[2] | **Xiaosong Bai**[1] | **Tianhang Qi**[3] | **Zhiyong Wei**[3] | **Ruichao Liu**[1] | **Keke Yin**[2] | **Jinxing Gao**[1] | **Daoyuan Yang**[1] | **Guangchao Zheng**[4] | **Johan E. ten Elshof**[5] | **Chongxin Shan**[4] | **Qi-Jun Sun**[6] | **Huiyu Yuan**[1,2]

[1] Henan Key Laboratory of High Temperature Functional Ceramics, School of Materials Science and Engineering, Zhengzhou University, Zhengzhou, China

[2] Henan Institute of Product Quality Supervision and Inspection, Zhengzhou, China

[3] Jiangsu Key Laboratory for Design & Manufacture of Micro/Nano Biomedical Instruments and School of Mechanical Engineering, Southeast University, Nanjing, China

[4] Key Laboratory of Material Physics, Ministry of Education, School of Physics and Microelectronics, Zhengzhou University, Zhengzhou, China

[5] MESA+ Institute for Nanotechnology, University of Twente, Enschede, The Netherlands

[6] State Key Laboratory of Terahertz and Millimeter Waves and Department of Materials Science and Engineering, City University of Hong Kong, Tat Chee Avenue, Kowloon, Hong Kong SAR, China

Correspondence
Chongxin Shan, Key Laboratory of Material Physics, Ministry of Education, School of Physics and Microelectronics, Zhengzhou University, Zhengzhou 450052, China.
Email: cxshan@zzu.edu.cn

Qi-Jun Sun, State Key Laboratory of Terahertz and MillimeterWaves and Department of Materials Science and Engineering, City University of Hong Kong, Tat Chee Avenue, Kowloon, Hong Kong SAR, China.
Email: qjsun2-c@my.cityu.edu.hk

Huiyu Yuan, Henan Key Laboratory of High Temperature Functional Ceramics, School of Materials Science and Engineering, Zhengzhou University, Zhengzhou 450001, China.
Email: hyyuan@zzu.edu.cn

Hao Liu and Bo Feng contributed equally to this work.

Abstract

Nanomaterials based pressure sensors have obtained world-wide research interest due to their promising potential applications in health monitoring, artificial intelligence, and electronic skin (e-skin). Despite the recent progress in sensitivity and detection range of the pressure sensors, the relatively high thickness of the active films has obstructed their applications for e-skin and degraded the comfortability as wearable devices. We hereby report for the first time a novel pressure sensor based on two-dimensional metal oxide nanosheets where the gaps between neighboring nanosheets are adjustable. The pressure sensors show a sensitivity of up to 7.2×10^6 kPa^{-1}, which is the highest value ever reported for a pressure sensor. Additionally, the sensor shows good repeatability and excellent stability. The pressure-sensing ranges can be tuned by adjusting the coverage of the nanosheet film. This work presents an effective strategy to develop ultrathin pressure sensors.

KEYWORDS
2D materials, pressure sensor, sensitivity, titanate nanosheets

Funding information
Young Top-notch Talent Program of Zhengzhou University, Grant/Award Number: 125/32310189; Science and Technology Program of Administration for Market Regulation of Henan Province, Grant/Award Number: 2020sj21; National Natural Science Foundation of China, Grant/Award Number: 51902290

1 | INTRODUCTION

Pressure sensing electronics are attracting extensive attention because of their potential applications in electronic skin (e-skin), touch-on flexible displays and health monitoring systems.[1–9] Nevertheless, the commercially available microelectromechanical systems (MEMS)-based pressure/tactile sensors have limited mechanical flexibility and pressure sensitivity, which obstructs their applications for many wearable and healthcare electronics. Alternatively, nanomaterials based pressure sensors have the merits of lightweight, low cost, easy fabrication, and large-scale compatibility, which make them a promising candidate as the building blocks for future electronics. According to the working principles, pressure sensors can be typically classified into the following four categories: Capacitive,[10,11] piezoresistive,[12–14] piezoelectric,[15–17] and triboelectric pressure sensors.[18–20] Among all these types of sensors, piezoresistive sensing devices have advantages of low cost, simple device construction and easy signal collection. Therefore, tremendous research efforts have been paid to the development of advanced piezoresistive pressure sensors.

Recently, various piezoresistive devices have been developed by the material selection and engineering.[13,21,22] These pressure sensors usually need complicated patterning processes.[22,23] Furthermore, the thickness of the sensing film is usually within the size of hundreds of micrometers or even several millimeters, which hinders the miniaturization of the devices. Furthermore, the piezoresistive pressure sensors generally function with electrical resistance change induced by the deformation of the conductive-film between electrodes (see Figure S1), and they suffer from low sensitivity. It is a great challenge to develop highly sensitive piezoresistive pressure sensors with small device thickness through a cost-effective approach. Two-dimensional (2D) oxides are a class of nanomaterials, including more than 30 members.[24] The 2D oxides are normally semiconducting or even insulating, flexible and highly stable;[24,25] Moreover, they are able to form monolayer nanosheet films by several techniques such as Langmuir-Blodgett deposition, spin coating and layer-by-layer assembly.[26–28] The 2D oxides are promising candidates for highly sensitive pressure sensors with limited device thickness. However, to the best of our knowledge, there is no report on the 2D oxide-based pressure sensors (2DOPSs) yet.

In this work, we report for the first time a novel pressure sensor based on the 2D oxides, and the demonstrated device functions with electrical resistance change induced by the deformation of the electrodes (see Figure S1b), demonstrating a novel sensing mechanism for the development of the piezoresistive pressure sensors. Even though the developed pressure sensor demonstrates a limited detection range, it shows an ultrahigh sensitivity in the order of 10^6 kPa^{-1} which occupies the highest value among all the reports. Furthermore, the pressure sensor can be easily integrated with other electronics in the future because of its simplicity in fabrication.

2 | RESULTS AND DISCUSSION

The device structure and working principle of the pressure sensor are illustrated in Figure 1. The device consists of two basic elements, indium tin oxide (ITO) coated polyethylene terephthalate (PET) electrodes and 2D oxide thin films (see Figure 1A). The working mechanism of the devices is illustrated in Figure 1B. When the device is free of pressure, the electrodes are separated by the 2D oxide thin films. However, the signal comes from contact between two electrodes when the device is under pressure. In this demonstration, we employed the 2D titanate nanosheet films which are found to be with a high dielectric constant of 125 and strong robustness even when the thickness of the nanofilm is down to 10 nm.[29] These 2D titanate films were fabricated by Langmuir-Blodgett (LB) deposition, and the thin film coverage and the layer number of the nanosheet films is easily controlled by the surface pressure in LB process.[27,30] Monolayer titanate films do not present diffraction peaks, but the diffraction peak appears when the layer number increases to 2 (Figure 1C). Raman spectra of the 2D titanate films (Figure 1D) present the characteristic peak at ~519 cm^{-m}, which is consistent with the previous report.[31] It is noted that the Raman data do not show an obvious shift as the layer changes

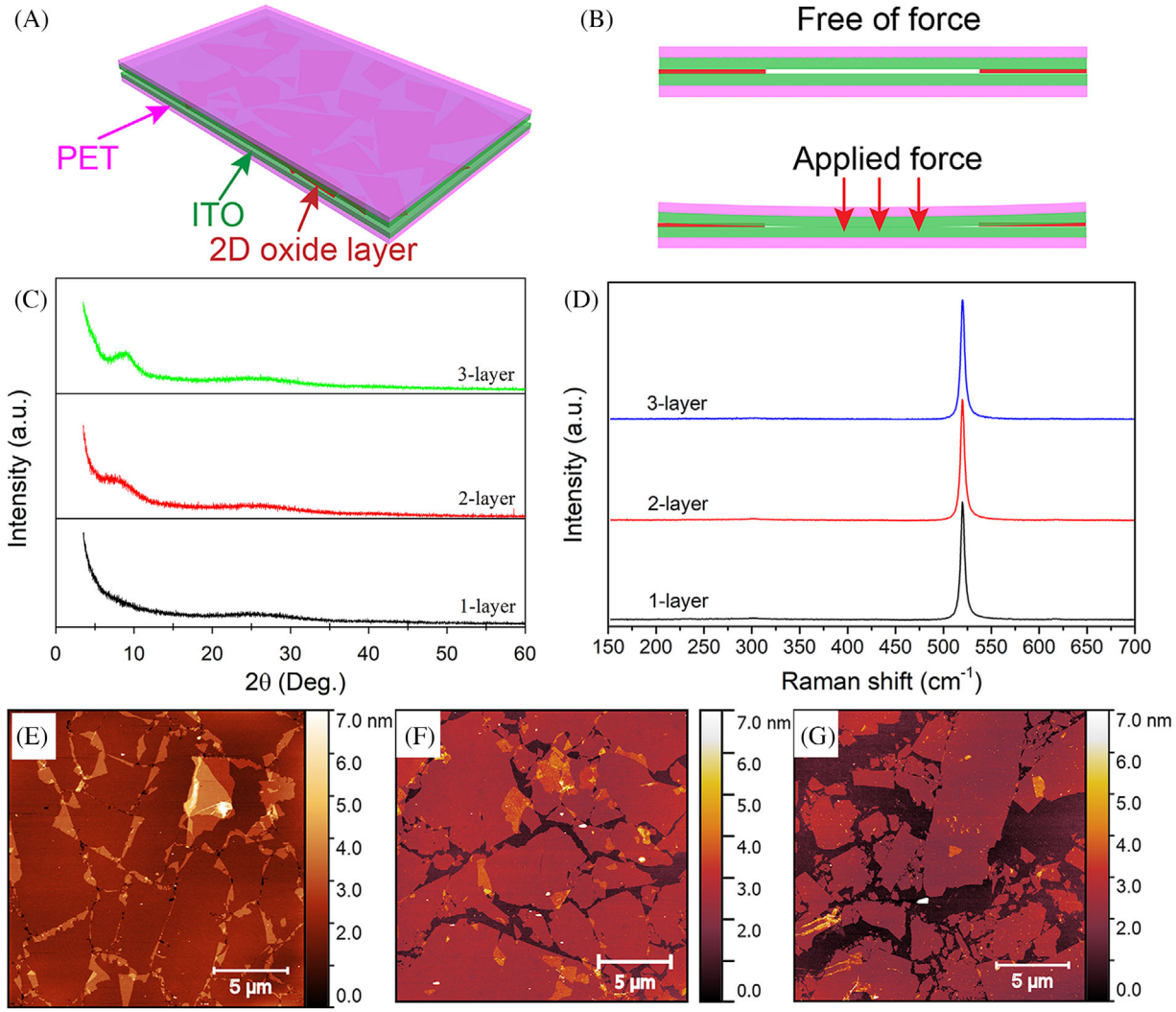

FIGURE 1 The schematic illustrations of (A) device structure and (B) working principle of the pressure sensor, (C) XRD patterns and (D) Raman spectra of the titanate nanosheet films with different layer, and AFM images of the titanate nanosheet film fabricated by LB deposition with (E) high coverage, (F) medium coverage and (G) low coverage

from 1 to 3 (Figure S2). The typical surface morphology of the titanate nanosheet films with different coverage on a smooth Si substrate is shown in Figure 1E-G. As shown in these figures, the 2D titanate thin films are always with gaps between neighboring nanosheets, even for the highly covered film. These gaps can serve as current paths when the pressure sensor is under the working pressure. The thickness of employed nanosheets in this work is 1.6 nm (Figure S3), and this value is slightly bigger than the commonly found value in the previous literature because of the high degree of adsorption of surfactant molecules on the nanosheet surface at the short reaction time.[32]

Figure 2A demonstrates the process of device fabrication. The 2D titanate nanosheets were obtained by exfoliation of the layered titanate in aqueous solution, the successful exfoliation yielded monolayer nanosheets which is confirmed by TEM data (Figure 2B), and then the nanosheets were transferred to an ITO/PET substate for device assembly. Figure 2C shows a complete device after all the processes. The morphology of the nanosheet films on the ITO/PET substrate was characterized by SEM and the typical results for samples are shown in Figure 2D and 2E. Figure 2D shows the SEM image of a boundary area of the nanosheet film. It can be seen that the empty area is brighter than the area covered by nanosheets. Figure 2E shows the magnified image of the boundary area, and the nanosheets distribute homogeneously on the substrate with gaps between them (see contrast modified images in Figure S4). The SEM images can also be found in Figure S4 to acquire the details of the gaps in the highly covered area. The gaps can be controlled with the LB process, and the distribution of the gaps could be controlled by the operating surface pressure. Readers who are interested in the details are encouraged to review the reference.[27,30]

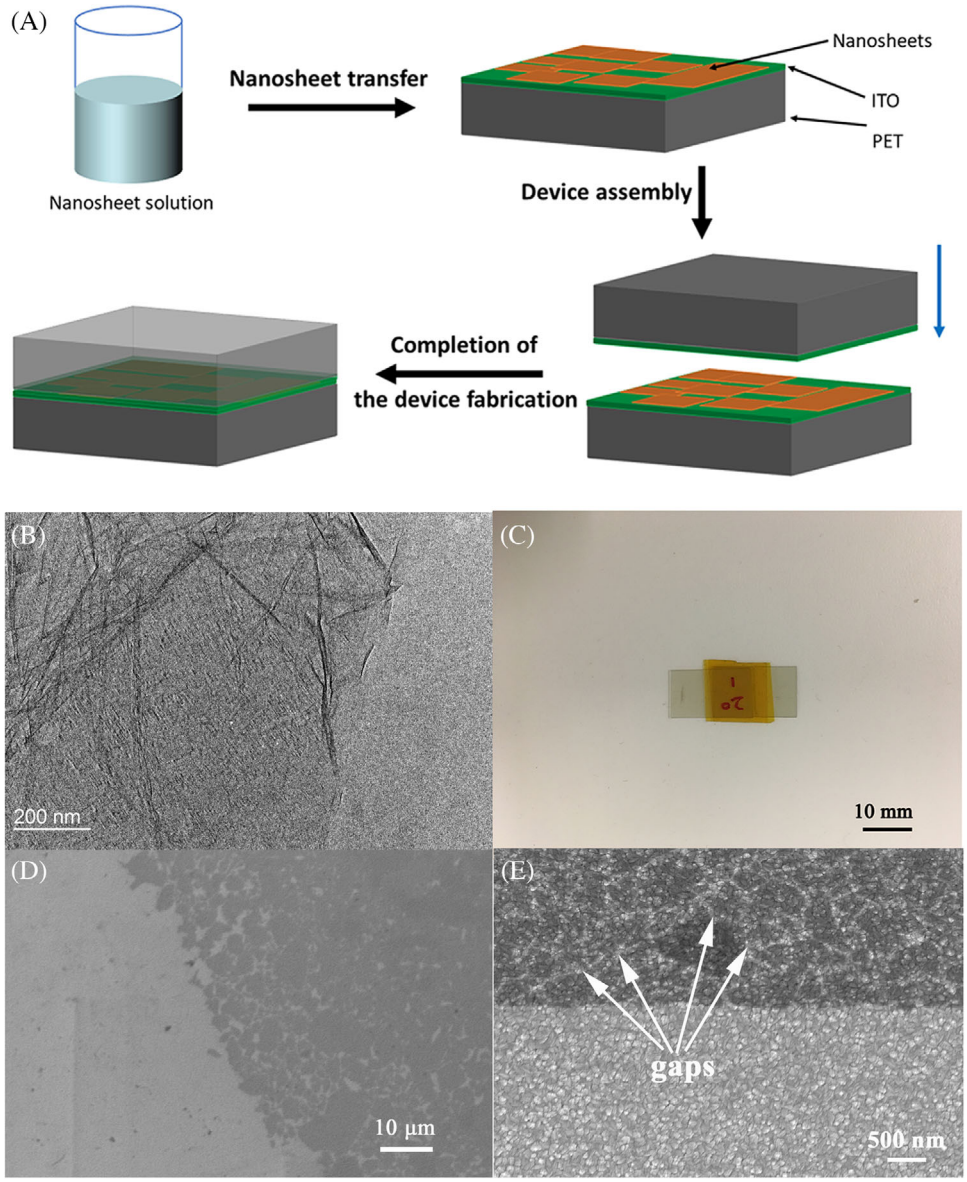

FIGURE 2 A, The schematic illustration of the device fabrication process, (B) TEM image of 2D titanate nanosheets, (C) Photograph of a typical device assembled, The typical SEM images of the 2D titanate nanosheets deposited on ITO/PET substrates: (D) the boundary area and (E) the magnified image of the boundary area

We assembled devices based on three samples, 2DOPS-L, 2DOPS-M and 2DOPS-H, which are fabricated under different LB process conditions to obtain different coverage, and their sensing performance is shown in Figure 3A. Without external pressure, the initial current is at a limited level, When external pressures were applied to the sensors, the devices showed a threshold pressure (P_{Th}) as shown in Figure 3A. Below the P_{Th}, the pressure sensors showed a negligible pressure sensitivity. However, when the applied pressure reached the threshold, the devices showed a high sensitivity in detecting the external pressure. The sensitivity (S) is defined as $S = \delta(\Delta I/I_0)/\delta P$, where ΔI, I_0 and P represent the change of current under external pressure, initial current, and applied pressure respectively. The three devices demonstrated different P_{Th} and ultrahigh sensitivity. The different coverage yielded the devices different P_{Th}, that is, 0.23, 1.49 and 2.84 kPa for the 2DOPS-L, 2DOPS-M and 2DOPS-H, respectively. Their sensitivity values were calculated to be 7.2×10^6, 1.5×10^6, and 8.0×10^5 kPa^{-1}, respectively, which is much higher than those of the recently reported piezoresistive pressure sensors (see Table 1). The devices showed different working ranges, and the working ranges were 0.23-0.40 (0.17), 1.49-2.02 (0.53) and 2.84-4.01(1.17) for 2DOPS-L, 2DOPS-M and 2DOPS-H, respectively. The high sensitivity is also demonstrated in Movie S1. It is clear that the lowering the

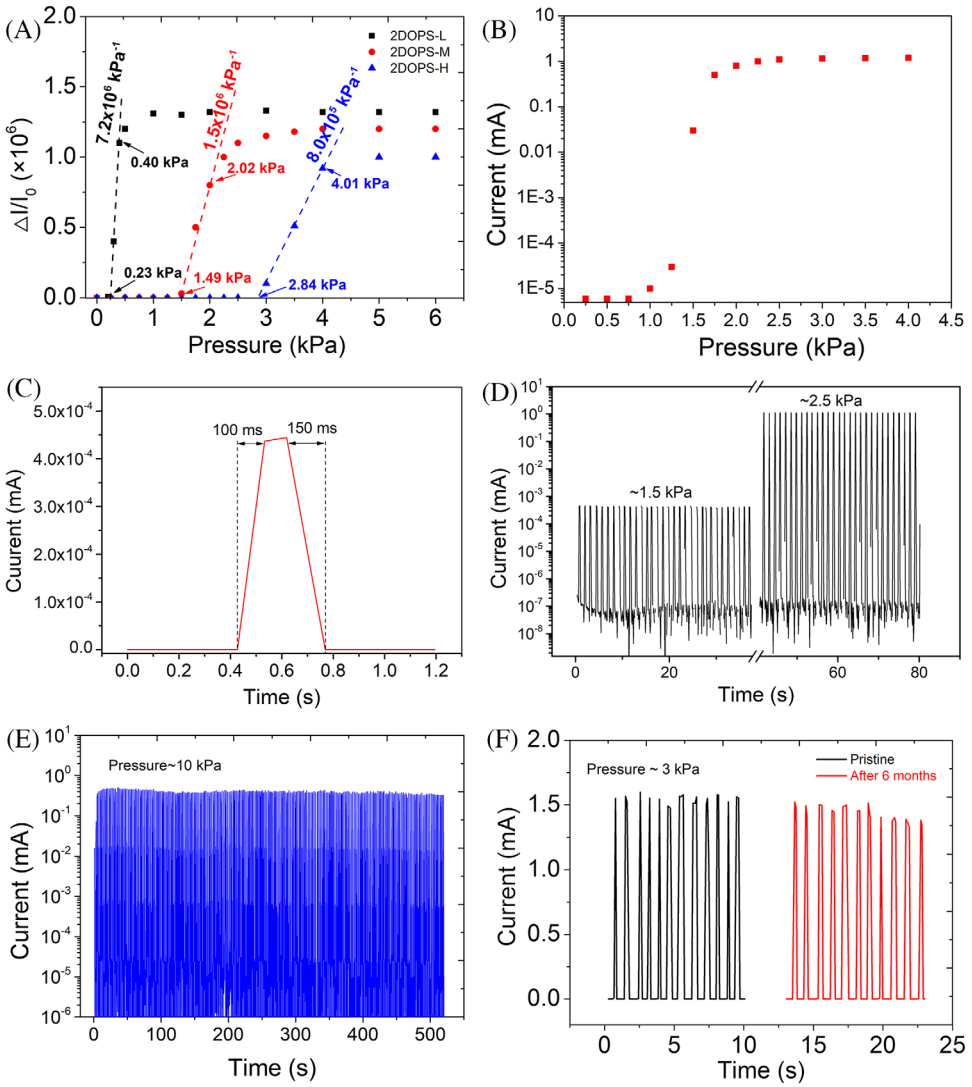

FIGURE 3 A, Sensing behavior of the 2DOPSs, (B) The detailed sensing behavior of the 2DOPS-M around PTh, (C) response time and recovery time of 2DOPS-M under a loading pressure of 1.5 kPa, (D) Short-term durability of the 2DOPS-M device at the pressure of ~1.5 and ~2.5 kPa (E), Long-term durability of the 2DOPS device, and (F) Stability performance of the 2DOPS device

coverage is one of the effective approaches to increase the detection range, and other approaches of expanding the detecting range are still under investigation. The high sensitivity of our pressure sensor is attributed to the unique structure of the devices. The nanofilms serve as a spacer to separate the top and bottom ITO electrodes when the sensor is below the P_{Th}, enabling the sensor to be with an ultralow initial current in the level of 10^{-6} mA as shown in Figure 3B. On the other hand, the conductive pathways could be formed easily when the applied pressure is over P_{Th} because of the ultrathin nanosheets, resulting in the ultrahigh sensitivity. The linear relationship of the I-V curves under various pressures with a sweep voltage from 0 to 1 V, as shown in Figure S5, provides a piece of convincing evidence for our hypothesis.

The response time is a very important factor for a pressure sensor and we conducted a measurement of the response time of 2DOPS-M under a loading pressure of 1.5 kPa, and the response time and recovery time were 100 and 150 ms, respectively. We also thoroughly investigated the device repeatability. Figure 3D shows the short-term repeatability performance under different pressures (~1.5 and ~2.5 kPa). Our sensor exhibited a good durability with a high signal-to-noise ratio. More importantly, the device also showed good long-term durability as shown in Figure 3E. These results suggest that the ultrathin nanosheets are robust and stable enough to operate in the devices. We also tested the device stability by re-testing the device after 6 months of fabrication and the results are shown in Figure 3F. It can be found that the device performance

TABLE 1 A, comparison of the pressure sensor in this paper with these reported

Pressure sensor	Materials	Sensitivity [kPa^{-1}]	Pressure range [kPa]	Reference
2DOPS	Monolayer titania nanosheets	1.5×10^6	1.49-2.02	This work
SWNTs/PDMS	single-walled carbon nanotubes	1.8	0.6×10^{-3}-0.3	[33]
AuNWs	ultrathin gold nanowires	1.14	0-5	[34]
Pyramid microstructure	SWCNTs/PDMS	2760.4	0-0.4	[22]
		8655.6	0.4-0.9	
		1874.5	0.9-1.2	
Au/microstructured PDMS	Au coated PDMS	50.17	0-0.07	[35]
		1.38	0.2-1.5	
rGO wrinkles	rGO	47.5	0-0.1	[36]
		178.5	0.1-0.2	
		43.9	0.2-0.5	
		7.94	0.5-3	
Biomimetically textured porous	PDMS/CNT	83.858	0-0.14	[37]
		0.400	0.14-10	
All-textile	Ni coated CNT Fabric	14.4	0-3.5	[38]
		7.8	3.5-15	
microstructured PDMS/polypyrrole	microstructured PDMS/polypyrrole	1907.2	0-0.1	[3]
		461.5	0.1-1.0	

was identical to the initial performance, indicating that the 2DOPS device is with excellent stability. We also tested the bendability of the devices, and we found that the devices can easily reach the saturate values under bending (see Movie S2). The saturate angel was ~5°.

In order to understand the details of the devices with different coverage under pressure, the finite element analysis was employed to simulate the deformation of the materials shown in Figure 4. When the gap is small (e.g., 50 nm), the deformation at the gap is small, and the main deformation occurs around the gap (Figure 4a), when the gap becomes bigger, the deformation becomes concentrated at the gap (Figures 4B-4H). The deformation also becomes larger when the gap becomes bigger under the same pressure (Figure 4I). These results explain well the sensing behavior of the devices with different coverage. When the coverage was small and the gaps were big (~2 μm), the electrodes were easy to deform and to connect with each other so the device showed a small P_{Th} and a higher sensitivity, When the coverage was high and the gaps were small (~ 150 nm), the electrodes needed higher pressure to deform and the deformation was not concentrated at the gaps, so the device showed a higher P_{Th} and lower sensitivity. The finite element analysis was also used to study the effect of the randomly distributed gaps on the sensing behavior, gaps with different size and shape on device under constant pressure were simulated, and the results are shown in Figure S6. The simulation demonstrates that, larger diameter gaps deform more under the same load for the same shape gaps (circle and square shape) which is consistent with the previous simulation, for a triangle shape gap, the acute-angle part of the gap deforms less, and the main deformation is concentrated in the center of the gap.

To demonstrate the potential of our 2DOPS for the application in health monitoring devices, we attached the sensor to a human wrist to detect the heartbeat rate in real-time. Figure 5 shows a demonstration of the 2DOPS device for heartbeat rate monitoring and the real-time current responses of the sensor to the heart beat rate of the volunteer. From the obtained waveforms, the average heartbeat rate is determined to be 60 beats per minute, which is identical to the measurement result by using a commercial medical device.

Although piezoresistive pressure sensors have been intensively studied for decades, a piezoresistive pressure sensor functioning with the ultrathin 2D oxide films is reported for the first time. The sensors, that is, 2DOPSs, rely on a monolayer 2D oxide thin film and demonstrate an ultrahigh sensitivity because of its unique structure. Even though a single 2DOPS shows a relatively small detecting range, they are promising to integrate into a multilayer sensing system for wide range sensing purpose considering the feature of adjustable pressure sensing range.

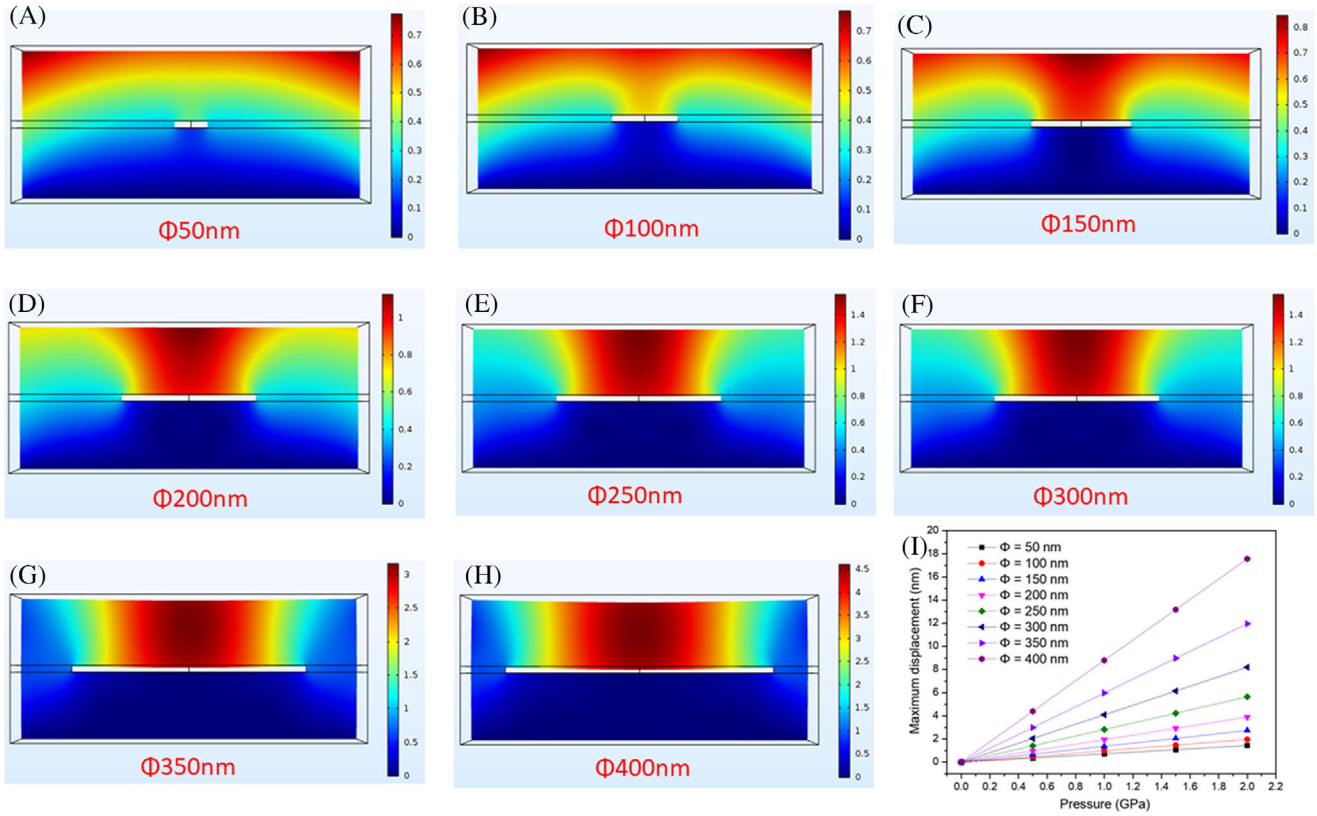

FIGURE 4 Deformation of the electrodes at the gap with the diameter of (A) 50 nm, (B) 100 nm, (C) 150 nm, (D) 200 nm, (E) 250 nm, (F) 300 nm, (G) 350 nm, (H) 400 nm under constant pressure simulated by finite element analysis, and (I) maximum displacement under different pressures for the gap with different size

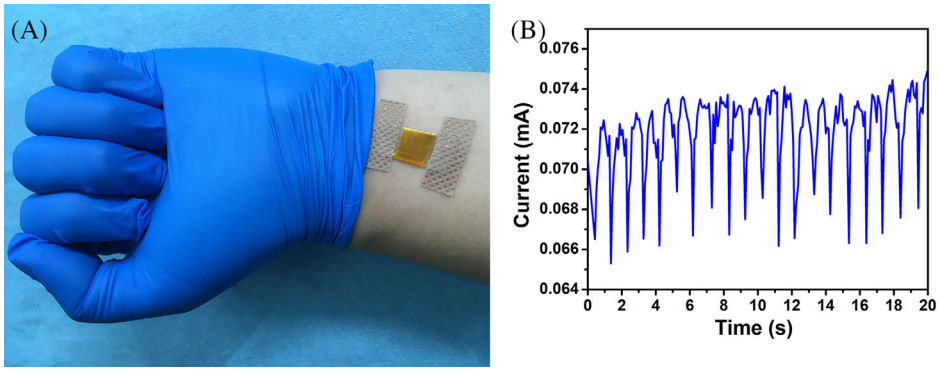

FIGURE 5 A, A demonstration of the 2DOPS for heart rate monitoring, (B) Heartbeat rate monitoring using the fabricated 2DOPS

3 | CONCLUSIONS

In conclusion, we have demonstrated a novel piezoresistive pressure sensor based on 2D oxides. The pressure sensors show an ultrahigh-pressure sensitivity, good repeatability and excellent stability. The detection range can be tuned by controlling the nanofilms coverage on the ITO electrode. Additionally, the sensor is easy to fabricate and no complicated patterning process is required. The results reported in this paper may provide an effective strategy to development of ultrahigh sensitive pressure sensors.

4 | EXPERIMENTAL SECTION

4.1 | Fabrication of 2D titanate thin films

The 2D titanate was obtained by exfoliation of layered titanate crystals $H_{1.07}Ti_{1.73}O_4$ (HTO) as described in

previous reports.[30,31,39] In brief, HTO crystals were firstly synthesized by immersing layered titanate crystals of $K_{0.80}Li_{0.27}Ti_{1.73}O_4$, which were at 1150°C obtained by sintering the mixture of K_2CO_3, Li_2CO_3 and TiO_2 in stoichiometric ratio, in 1 M HNO_3 aqueous solution for 3 days, while the acid solution was refreshed daily to achieve complete protonation. After the protonation was completed, the white HTO crystals were filtered, washed and air-dried. Then, 0.1 g HTO crystals were mixed with tetrabutylammonium hydroxide (TBAOH) to achieve exfoliation, and the reaction time was 1 day.

When the solution was ready, 2 ml solution containing 2D titanate nanosheets was taken and diluted into 500 ml for LB deposition. Before the LB deposition process, ITO/PET substrates were cleaned by DI-water and ethanol, respectively. When the substrate was ready, it was immersed in the diluted solution which was stabilized for 10 minutes, and the LB deposition started. The surface pressure was controlled to be ~3.0, ~5.0, and ~11.0 mN m^{-1}, respectively. The surface pressure directly determines the coverage. The samples fabricated under the above surface pressures were denoted as 2DOPS-L, 2DOPS-M and 2DOPS-H, respectively.

4.2 | Device assembly and test

The pressure sensor devices with a sandwiched structure were assembled by using an ITO/PET substrate (10 mm x 15 mm) and nanofilm coated ITO/PET substrate (10 mm x 15 mm) with the assistance of polyimide tapes, and the overlapping area was 10 mm x 10 mm. Copper wires were attached onto the top and bottom ITO electrodes for external measurement connection. The current to pressure response of the devices was performed with a test stand connected with a force gauge. The applied voltage was 1 V, and the electrical signals were collected by a Keithley 2612A analyzer. We tested the pressure sensor for heart rate monitoring in a single healthy human (first corresponding author) whose consent was obtained prior to the measurement, and no approval from the national or institutional ethics board/committee was required to conduct heart rate measurements with a pressure sensor for research purpose.

4.3 | Characterization

Tapping mode Atomic Force Microscopy (AFM, Flyingman Nanoview 6800) was used to determine the height profile of 2D titanate nanosheets deposited on Si wafers. The AFM data were further analyzed using the Gwyddion software package. Transmission electron microscopy (TEM, Joel JEM-2100F) was used to visualize the nanosheets. Scanning electron microscopy (SEM, Zeiss EVO HD15) was used to observe the morphology of samples. X-ray diffraction patterns of all the thin film samples were acquired by a Philips X′Pert X-ray diffractometer (Cu Kα radiation with a wavelength of 0.15405 nm). Raman spectra were collected with a Jobin-Yvon LabRAM Horiba Raman spectrometer, and the laser wavelength and energy were 532 nm and 1.8 mW, respectively.

4.4 | Simulation details

The finite element method is performed to calculate the deformation of the sensor with various structural parameters. To simplify the calculation, the model is composed of three parts with the same in-plane size of 500 × 500 nm^2. Both the upper and lower layers are ITO with a thickness of 100 nm. The middle layer is potassium lithium titanate ($K_{0.8}Li_{0.27}Ti_{1.73}O_4$) with a thickness of 10 nm. The gap between the potassium lithium titanate in the real sample is modeled by a circular pore in the center of the middle layer with various diameters from 50 to 400 nm. Multiple gaps with different size and shape are simulated to analyze the sensing behavior of the devices with randomly distributed gaps. Before the calculation, the Poisson's ratio, Young's modulus and density of ITO are set as 0.35,[40] 140 GPa[41] and 7.15 g cm^{-3}, respectively. But the mechanical properties of the nanoscale potassium lithium titanate have rarely been studied. Thus, the mechanical parameters of bulk titanium dioxide are used instead. The Poisson's ratio, Young's modulus and density of the potassium lithium titanate[42] are set as 0.27, 230 GPa and 4.23 g cm^{-3}, respectively. During the calculation, all the three layers were set as a linear elastic material, and the initial values of the displacement field and the structural velocity field are zero. The bottom of the lower layer is fixed and the load is applied uniformly on the top of the upper layer.

ACKNOWLEDGMENTS

The authors acknowledge the financial support of the Young Top-notch Talent Program of Zhengzhou University (No. 125/32310189), the Science and Technology Program of Administration for Market Regulation of Henan Province (2020sj21), and the National Natural Science Foundation of China (No. 51902290). H. Yuan acknowledges Prof. Dr. Shawn Zhang for the language polishing.

DATA AVAILABILITY STATEMENT

Research data are not shared.

REFERENCES

1. W. Yuan, J. Yang, K. Yang, H. Peng, F. Yin, *ACS Appl. Mater. Interfaces* **2018**, *10*, 19906.
2. S. H. Kim, S. Jung, I. S. Yoon, C. Lee, Y. Oh, J.-M. Hong, *Adv. Mater.* **2018**, *30*, 1800109.
3. H. Li, K. Wu, Z. Xu, Z. Wang, Y. Meng, L. Li, *ACS Appl. Mater. Interfaces* **2018**, *10*, 20826.
4. S.-J. Park, J. Kim, M. Chu, M. Khine, *Adv. Mater. Technol.* **2016**, *1*, 1600053.
5. Y. Lee, J. Park, S. Cho, Y.-E. Shin, H. Lee, J. Kim, J. Myoung, S. Cho, S. Kang, C. Baig, H. Ko, *ACS Nano* **2018**, *12* (4), 4045.
6. Q.-J. Sun, T. Li, W. Wu, S. Venkatesh, X.-H. Zhao, Z.-X. Xu, V. A. L. Roy, *ACS Appl. Electron. Mater.* **2019**, *1*, 711.
7. Q.-J. Sun, X.-H. Zhao, Y. Zhou, C.-C. Yeung, W. Wu, S. Venkatesh, Z.-X. Xu, J. J. Wylie, W.-J. Li, V. A. L. Roy, *Adv. Funct. Mater.* **2019**, *29*, 1808829.
8. Q.-J. Sun, J. Zhuang, S. Venkatesh, Y. Zhou, S.-T. Han, W. Wu, K.-W. Kong, W.-J. Li, X. Chen, R. K. Y. Li, V. A. L. Roy, *ACS Appl. Mater. Interfaces* **2018**, *10*, 4086.
9. Z. Lou, S. Chen, L. Wang, K. Jiang, G. Shen, *Nano Energy* **2016**, 7.
10. Y. Luo, J. Shao, S. Chen, X. Chen, H. Tian, X. Li, L. Wang, D. Wang, B. Lu, *ACS Appl. Mater. Interfaces* **2019**, *11*, 17796.
11. X. Shuai, P. Zhu, W. Zeng, Y. Hu, X. Liang, Y. Zhang, R. Sun, C.-p. Wong, *ACS Appl. Mater. Interfaces* **2017**, *9*, 26314.
12. K.-H. Kim, S. K. Hong, N.-S. Jang, S.-H. Ha, H. W. Lee, J.-M. Kim, *ACS Appl. Mater. Interfaces* **2017**, *9*, 17499.
13. X.-H. Zhao, S.-N. Ma, H. Long, H. Yuan, C. Y. Tang, P. K. Cheng, Y. H. Tsang, *ACS Appl. Mater. Interfaces* **2018**, *10*, 3986.
14. B. Zhu, Z. Niu, H. Wang, W. R. Leow, H. Wang, Y. Li, L. Zheng, J. Wei, F. Huo, X. Chen, *Small* **2014**, *10*, 3625.
15. J. Chun, N.-R. Kang, J.-Y. Kim, M.-S. Noh, C.-Y. Kang, D. Choi, S.-W. Kim, Z. L. Wang, J. M. Baik, *Nano Energy* **2015**, *11*, 1.
16. J. Li, S. Chen, W. Liu, R. Fu, S. Tu, Y. Zhao, L. Dong, B. Yan, Y. Gu, *J. Phys. Chem. C* **2019**, *123*, 11378.
17. S. Cheon, H. Kang, H. Kim, Y. Son, J. Y. Lee, H.-J. Shin, S.-W. Kim, J. H. Cho, *Adv. Funct. Mater.* **2018**, *28* (2), 1703778.
18. F.-R. Fan, L. Lin, G. Zhu, W. Wu, R. Zhang, Z. L. Wang, *Nano Lett.* **2012**, *12*, 3109.
19. K. Y. Lee, H.-J. Yoon, T. Jiang, X. Wen, W. Seung, S.-W. Kim, Z. L. Wang, *Adv. Energy Mater.* **2016**, *6* 1502566.
20. X. Pu, M. Liu, X. Chen, J. Sun, C. Du, Y. Zhang, J. Zhai, W. Hu, Z. L. Wang, *Sci. Adv.* **2017**, *3*, e1700015.
21. S. C. B. Mannsfeld, B. C. K. Tee, R. M. Stoltenberg, C. V. H. H. Chen, S. Barman, B. V. O. Muir, A. N. Sokolov, C. Reese, Z. Bao, *Nat. Mater.* **2010**, *9*, 859.
22. Z. Huang, M. Gao, Z. Yan, T. Pan, S. A. Khan, Y. Zhang, H. Zhang, Y. Lin, *Sensor. Actuat. A-Phys.* **2017**, *266*, 345.
23. Y. Zhang, Y. Hu, P. Zhu, F. Han, Y. Zhu, R. Sun, C.-P. Wong, *ACS Appl. Mater. Interfaces* **2017**, *9*, 35968.
24. J. E. ten Elshof, H. Yuan, P. G. Rodriguez, *Adv. Energy Mater.* **2016**, *6*, 1600355.
25. K. Kalantar-zadeh, J. Z. Ou, T. Daeneke, A. Mitchell, T. Sasaki, M. S. Fuhrer, *Appl. Mater. Today* **2016**, *5*, 73.
26. T. Sasaki, Y. Ebina, T. Tanaka, M. Harada, M. Watanabe, G. Decher, *Chem. Mater.* **2001**, *13*, 4661.
27. M. Muramatsu, K. Akatsuka, Y. Ebina, K. Wang, T. Sasaki, T. Ishida, K. Miyake, M. Haga-a., *Langmuir* **2005**, *21*, 6590.
28. K. Matsuba, C. Wang, K. Saruwatari, Y. Uesusuki, K. Akatsuka, M. Osada, Y. Ebina, R. Ma, T. Sasaki, *Sci. Adv.* **2017**, *3*.
29. M. Osada, Y. Ebina, H. Funakubo, S. Yokoyama, T. Kiguchi, K. Takada, T. Sasaki, *Adv. Mater.* **2006**, *18*, 1023.
30. H. Yuan, R. Lubbers, R. Besselink, M. Nijland, J. E. ten Elshof, *ACS Appl. Mater. Interfaces* **2014**, *6*, 8567.
31. P. Sun, R. Ma, M. Osada, T. Sasaki, J. Wei, K. Wang, D. Wu, Y. Cheng, H. Zhu, *Carbon* **2012**, *50*, 4518.
32. H. Yuan, M. Timmerman, M. van de Putte, P. Gonzalez Rodriguez, S. Veldhuis, J. E. ten Elshof, *J. Phys. Chem. C* **2016**, *120*, 25411.
33. X. Wang, Y. Gu, Z. Xiong, Z. Cui, T. Zhang, *Adv. Mater.* **2014**, *26*, 1336.
34. S. Gong, W. Schwalb, Y. Wang, Y. Chen, Y. Tang, J. Si, B. Shirinzadeh, W. Cheng, *Nat. Commun.* **2014**, *5*, 3132.
35. B. Su, S. Gong, Z. Ma, L. W. Yap, W. Cheng, *Small* **2015**, *11*, 1886.
36. J. Jia, G. Huang, J. Deng, K. Pan, *Nanoscale* **2019**, *11*, 4258.
37. T. Zhao, T. Li, L. Chen, L. Yuan, X. Li, J. Zhang, *ACS Appl. Mater. Interfaces* **2019**, *11*, 29466.
38. M. Liu, X. Pu, C. Jiang, T. Liu, X. Huang, L. Chen, C. Du, J. Sun, W. Hu, Z. L. Wang, *Adv. Mater.* **2017**, *29*, 1703700.
39. H. Yuan, D. Dubbink, R. Besselink, J. E. ten Elshof, *Angew. Chem. Int. Ed.* **2015**, *54*, 9239.
40. D. G. Neerinck, T. J. Vink, *Thin Solid Films* **1996**, *278*, 12.
41. N. Biswas, P. Ghosh, S. Sarkar, D. Moitra, P. K. Biswas, S. Jana, A. K. Mukhopadhyay, *Thin Solid Films* **2015**, *579*, 21.
42. B. Huang, *Comprehensive Dictionary of Materials*. 2nd ed., Chemical Industry Press: **2016**.

SUPPORTING INFORMATION

Additional supporting information may be found online in the Supporting Information section at the end of the article.

How to cite this article: H. Liu, B. Feng, X. Bai, T. Qi, Z. Wei, R. Liu, K. Yin, J. Gao, D. Yang, G. Zheng, J. E. ten Elshof, C. Shan, Q.-J. Sun, H. Yuan, *Nano Select* **2021**, 1.
https://doi.org/10.1002/nano.202100053